Finite molecular anchoring in the escaped-radial nematic configuration: A ^{2}H-NMR study

G. P. Crawford, D. W. Allender, and J. W. Doane
Liquid Crystal Institute and Department of Physics, Kent State University, Kent, Ohio 44242-0001

M. Vilfan and I. Vilfan
J. Stefan Institute, University of Ljubljana, 61111 Ljubljana, Yugoslavia
(Received 30 January 1991; revised manuscript received 3 May 1991)

The director-field configuration of a nematic liquid crystal confined to cylindrical cavities of polycarbonate Nuclepore membranes ranging from 0.3 to 0.05 μm in radius is determined using deuterium nuclear magnetic resonance (^{2}H NMR). Spectral patterns from cavities of radius 0.3 μm reveal the escaped-radial configuration with singular point defects, but as the cylinder size is decreased, the elastic energy imposed by the curvature of the confining walls competes with the anchoring energy to tilt the directors away from their preferred perpendicular anchoring direction, preventing the expected transition to the planar-radial configuration. A surface fitting parameter is directly determined by simulating ^{2}H-NMR line shapes, and by studying a series of samples with different radii, the molecular-anchoring strength W_0 and surface elastic constant K_{24} are extracted.

I. INTRODUCTION

The existence of the escaped-radial configuration for a nematic liquid crystal confined in cylindrical cavities with perpendicular boundary conditions was first proposed by Cladis and Kleman [1] and Meyer [2] for cylinder radii larger than ~ 0.1 μm. The escaped-radial director field is planar radial near the cylinder walls, and bends out of the plane to escape along the axis of the cylinder. This has been optically verified in large cylinders of radii 20–200 μm [2–4]. The presence of singular point defects along the cylinder axis was also revealed resulting from the fact that two energy-equivalent configurations exist where the direction of bend is changed [3–7]. It was further predicted that the escaped-radial configuration will revert to the planar-radial configuration with a line disclination at $R_c \sim 0.1 \mu$m [1,2]. This configuration was further explored theoretically by Lin, Palffy-Muhoray, and Lee [8]. Recently, the NMR technique was used to experimentally study these structures confined to submicrometer size cylindrical cavities [9]. ^{2}H-NMR spectral patterns revealed the escaped-radial configuration with singular point defects present along the cylinder axis in cavities 0.3 μm in radius. These spectra were used to determine the density of singular point defects in the strong-anchoring limit.

In this contribution we investigate the effect of weak anchoring strengths and high curvature on nematic-liquid-crystal configurations that become important in small cavities. We have studied cylindrical cavities ranging in size from 0.3 to 0.05 μm in radius, where the anchoring strength and surface elastic constant K_{24} become sensitive to the NMR technique. ^{2}H-NMR spectral patterns are recorded for parallel and perpendicular orientations of the cylinder axis in the magnetic field to determine the nematic director distribution inside the cavities. Simulations of these patterns were then numerically calculated for the escaped-radial configuration with singular point defects to determine both the molecular-anchoring strength and the surface elastic constant (K_{24}) by measuring an effective anchoring strength directly from the ^{2}H-NMR spectrum.

The molecular-anchoring strength W_0 is one of the most important interfacial parameters that characterizes the interaction between an elongated liquid-crystal molecule and the solid substrate; it is useful in understanding the operation of many liquid-crystal devices. There are various experimental techniques for measuring W_0 on planar surfaces; they can be categorized as either geometry-type [10] or external-field-type [11] techniques. The values of W_0 reported in the literature [12,13] for treated planar glass substrates range between 10^{-6} and 10^{-4} J/m^2 depending on the molecular orientation at the surface and the surface treatment employed. There has been only one measurement of W_0 reported in confined geometries [14]. Erdmann, Zumer, and Doane have investigated the radial-to-axial configuration transition in supramicrometer nematic droplets via optical microscopy, reporting values for W_0 of the order of 10^{-5} J/m^2 for a polyurethane binder. Observation of this transition by optical methods is limited to cavity radii ≥ 3 μm, usually larger than the size employed in liquid-crystal-based electro-optic devices [15,16]. The surface elastic constant K_{24} was not treated in these studies since the cavity sizes were comparatively large, resulting in the surface elastic term being negligible compared to the anchoring-strength term. ^{2}H-NMR extends these studies of finite-size effects to substantially smaller cavities, where optical methods become insensitive to the details of nematic structure inside the cavities.

The ^{2}H-NMR technique provides a direct indication of the nematic director configuration from the spectral distribution pattern. Spectral patterns reveal the profile of the structure for different orientation of the cylinder axis

projected along the magnetic-field direction of the NMR spectrometer, allowing for precise director-configuration determination. For surfaces to be accessible with ^{2}H-NMR, a system with a large surface-to-volume ratio must be realized. The cylindrical pores of polycarbonate Nuclepore membranes filled with a nematic liquid crystal exhibit these properties. These systems have been shown to be convenient systems in which to investigate finite-size effects [17], and have recently been used to study ordering and self-diffusion in the isotropic phase at a solid interface [18]. The intent of this contribution is to extend our earlier studies [9] to smaller cavity sizes, where the molecular-anchoring strength and surface terms in the Frank free energy become important.

II. THE EFFECT OF ANCHORING STRENGTH ON THE ESCAPED-RADIAL CONFIGURATION

A nematic liquid crystal confined to a cylindrical environment exhibits a specific director configuration resulting from an interplay between elastic forces, a possible external field, the morphology and size of the cavity, and surface interactions. The deformation free energy of a confined liquid crystal in the constant-order-parameter approximation can be expressed as

$$F=\frac{1}{2}\int_{\text{vol}}[K_{11}(\text{div}\mathbf{n})^2+K_{22}(\mathbf{n}\cdot\text{curl}\mathbf{n})^2+K_{33}(\mathbf{n}\times\text{curl}\mathbf{n})^2-K_{24}\text{div}(\mathbf{n}\times\text{curl}\mathbf{n}+\mathbf{n}\cdot\text{div}\mathbf{n})]dV$$
$$-\frac{1}{2}\int_{\text{vol}}\frac{\Delta\chi}{\mu_0}(\mathbf{B}\cdot\mathbf{n})^2dV+\frac{1}{2}\int_{\text{surf}}W_0\sin^2[\phi(R)-\phi_0]dS\ , \tag{1}$$

where $\mathbf{n}$ is the nematic director, the first three terms describe the splay, twist, and bend deformations, respectively, with K_{11}, K_{22}, and K_{33} denoting the appropriate elastic constants. The fourth term is a surface elastic contribution where K_{24} is a material constant independent of short-range interactions at the surface. The fifth term incorporates the effect of the magnetic field, with $\Delta\chi$ the diamagnetic susceptibility anisotropy. The final term is the anisotropic part of the surface free energy; W_0 is the molecular-anchoring strength, and ϕ_0 and $\phi(R)$ are the preferred and actual anchoring angles, respectively. A term proportional to the surface elastic constant K_{13} is neglected based on having weak deformation and consistently keeping terms only of first derivatives of $\mathbf{n}$. If K_{13} is to be included, other terms involving the square of the second derivatives of $\mathbf{n}$ must also be kept.

The influence of the magnetic field term in the free energy can be estimated by calculating the coherence length ξ_m, expressed by

$$\xi_m=\left[\frac{\mu_0 K}{\Delta\chi}\right]^{1/2}\frac{1}{B}\ , \tag{2}$$

where K can be either K_{11} or K_{33}, or some average of these elastic constants depending upon the specific director configuration. The NMR spectrometer has a magnetic field of 4.7 T, which produces a coherence length of ≈ 1.7 μm (for 4′-pentyl-4-cyanobiphenyl [19]) significantly larger than the radii of the cylindrical cavities studied here. Therefore the magnetic-field term has no appreciable influence on the nematic-director configuration. It was previously shown that even exaggerated values of the magnetic field ($B=26$ T) had no effect on the spectral-line-shape calculation for cavities of radius 0.3 μm [9].

Other authors [1,2] have minimized Eq. (1) assuming strong anchoring of the nematic director perpendicular to the cavity wall [$\phi(R)=\phi_0=\pi/2$] and avoiding twist deformation. In the absence of external-field effects and the surface elastic contributions, the resulting cylindrically symmetric equilibrium configuration in the approximation $K_{11}=K_{33}$ is expressed by

$$\phi(r)=2\tan^{-1}\left[\frac{r}{R}\right]\ , \tag{3}$$

where $\phi(r)$ is the angle between the nematic director and the cylinder axis, R is the cylinder radius, and r is the local position in cylindrical coordinates of the nematic director, i.e., the distance from the cylinder axis. This configuration is called the escaped-radial structure because the molecular orientation, which is planar radial near the walls, bends out of the plane to escape along the cylinder axis into the third dimension. Singular point defects frequently exist in cylindrically confined systems [3–7,9], and are of two types, radial and hyperbolic. They alternate along the axis of the cylinder and result from the fact that two energetically equivalent configurations exist with opposite direction of bend.

To treat the problem more realistically, and to obtain molecular-anchoring-strength information in submicrometer cylindrical cavities, the deviation of the nematic director at the surface must be included to incorporate the competition between elastic and surface anchoring energies. This is done by relaxing the boundary condition at the surface $\phi(R)=\pi/2$ to an initially undetermined angle $\phi(R)=\phi_R$, which results from the minimization of the free energy with the surface contribution term included. Performing a variational calculation, the equilibrium configuration in the approximation $K_{11}=K_{33}\neq K_{24}$ is obtained in closed-form expressed as

$$\tan\left[\frac{\phi(r)}{2}\right]=\frac{r}{R}\tan\left[\frac{\phi_R}{2}\right]\ . \tag{4}$$

The tilt angle that the director makes with the surface, ϕ_R, is given by the relation (valid for $\sigma\geq 1$)

$$\phi_R = \cos^{-1}\left[\frac{1}{\sigma}\right], \tag{5}$$

where σ is the effective anchoring strength given by the dimensionless expression

$$\sigma = \frac{RW_0}{K} + \frac{K_{24}}{K} - 1 . \tag{6}$$

This structure is presented in Fig. 1 for various values of σ. In the strong anchoring limit, $\sigma \to \infty$, resulting in $\phi_R \to \pi/2$, reducing Eq. (4) to Eq. (3) with strong anchoring assumed. In the case of very weak anchoring ($\sigma \leq 1$), where $\phi_R \to 0$, the configuration reduces to a parallel orientation along the cylinder axis with no surface effects. For intermediate anchoring energies and small cavity sizes, a case where the surface and elastic energies compete, the deviation of the anchoring angle becomes significant and must be incorporated.

Based on empirical observation [9], singular points defects exist in the submicrometer cavities in Nuclepore membranes at the encounter of two oppositely escaped domains. Point defects are included in the escaped-radial configuration by incorporating a planar-radial distribution of directors in planes a finite distance L apart. There is no analytic expression for $\phi(r)$ for the molecular distribution of this configuration. The resulting structure is numerically calculated by minimizing Eq. (1) in the approximation $K_{11} = K_{33} \neq K_{24}$ and presented in Fig. 2 for different values of σ. The radial planes of directors or domain walls carry an additional free energy due to the elastic deformations. It was calculated [20] that the interaction between domain walls is attractive for small L/R ($L/R \lesssim 0.25$) and repulsive for larger L/R. This implies that the domain walls will annihilate when they are closer than $L/R \approx 0.25$. For $L/R \gtrsim 0.25$ they will repel but cannot disappear at the open surface of the cylinder because of another repulsive interaction between the domain wall and the surface. Thus the structure with domain wall separation $L/R \gtrsim 0.25$ is (meta)stable.

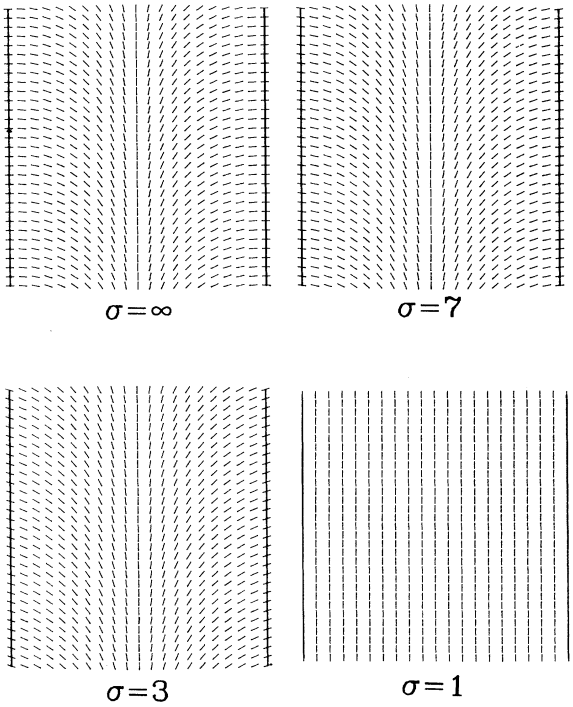

FIG. 1. Calculated nematic-director distributions in the one-constant approximation for different values of σ for the escaped-radial configuration.

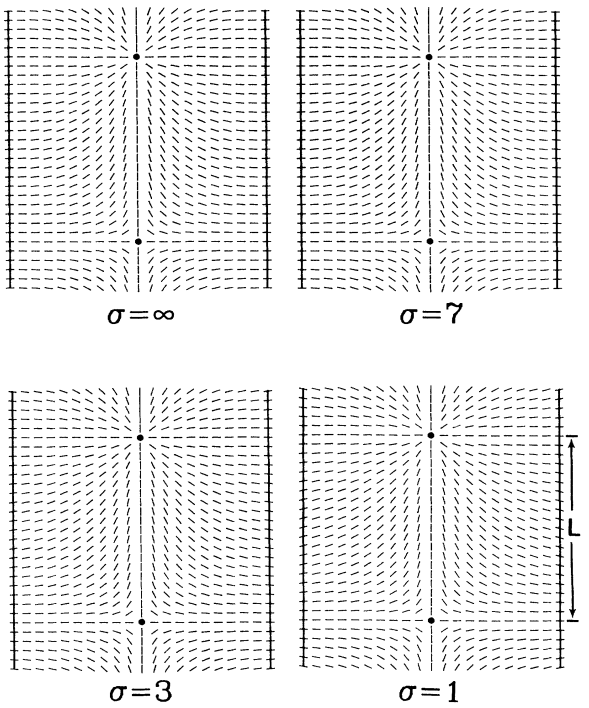

FIG. 2. Calculated nematic-director distributions in the one-constant approximation for different values of σ for the escaped-radial configuration with singular point defects, where L is the distance between successive point defects. The point defects which alternate along the cylinder axis are of the radial and hyperbolic type.

III. PRINCIPLE OF MOLECULAR-ANCHORING-STRENGTH MEASUREMENT VIA ^{2}H-NMR

The ^{2}H-NMR technique provides direct information on the effective molecular-anchoring strength given by Eq. (6) from the spectral pattern. The characteristic features of the spectral pattern that are important in our investigations depend on three factors: the nematic-director configuration inside the cylinder, the orientation of the cylinder with respect to the magnetic field, and molecular translational self-diffusion. When the effects of translational self-diffusion can be neglected, the ^{2}H-NMR spectral pattern is a direct indication of the nematic-director configuration in the cylinder because the resonance frequency depends on the angle between the nematic director and the external field. The advantage of

cylindrically dispersed liquid crystals over the spherical geometries [21] employed in polymer dispersed liquid-crystal devices [14-16] is the ability to change the orientation of the cylinder in the magnetic field. This allows the profile of the configuration to be projected in different directions for better structure determination. By simulating the spectral distribution for different profiles and varying the cavity size, the molecular-anchoring strength can be determined.

The ^{2}H-NMR spectral pattern is dominated by the quadrupole interaction of the deuterium nucleus (spin $I=1$) with the electric-field gradient of the carbon–deuterium bond [22]. A uniaxial liquid crystal compound selectively deuterated will yield a spectrum of two lines at angular quadrupole frequencies given by

$$\omega_q(\mathbf{r})=\pm\pi\frac{\delta\nu_B}{2}[3\cos^2\theta(\mathbf{r})-1]\ , \tag{7}$$

where $\theta(\mathbf{r})$ is the angle between the magnetic field $\mathbf{B}$ and the local nematic director $\mathbf{n}(\mathbf{r})$, and $\delta\nu_B$ is the quadrupole splitting of an aligned bulk nematic. In the case where the magnetic field macroscopically aligns the nematic liquid crystal, only two absorption lines are present. In our situation, there is a distribution of frequencies that reflects the configuration of the directors in the cylinder.

The spectral distribution is calculated from the free-induction decay (FID) which is a relaxation function describing the nuclear magnetization in the time domain. Dividing the time interval $(0,t)$ into equal parts, the FID can be expressed as [23]

$$G(t)=\left\langle \exp\left[i\int_0^t\omega_q(\mathbf{r}(t'))dt'\right]\right\rangle$$
$$=\sum_j \exp[i\omega_q(r_j)t]P(r_j)\ , \tag{8}$$

where $\langle\ \rangle$ represents an ensemble average, ω_q is defined by Eq. (6), and P is the time-independent probability of having a molecule with frequency $\omega_q(r_j)$ at position r_j. The frequency spectrum is obtained by the Fourier transformation of Eq. (8), given by

$$I(\omega_q)=\int_{-\infty}^{\infty}G(t)\exp(-i\omega_q t)dt\ . \tag{9}$$

Line broadening is taken into account by convoluting $I(\omega_q)$ with a Gaussian distribution function. For cylinder sizes of the order of the spatial dimension of diffusion, the influence of motional averaging must be taken into account. This can be done by considering an instantaneous value of the quadrupole frequency and time-dependent probability in Eq. (8). The extent of motional averaging can be estimated by comparing the range that the molecule diffuses on the NMR time scale, $d\sim\sqrt{D/\delta\nu}$, to the distance where the director orientation changes appreciably. Using typical values of the diffusion constant $D\sim10^{-11}$ m^2/s, and the quadrupole splitting frequency of a macroscopically aligned bulk nematic sample $\delta\nu\sim40$ kHz, the range that a molecule migrates is $d\sim0.02$ μm, which is much less than the cavity sizes in this study. Therefore only minor effects of diffusion can be expected [9].

To illustrate the effect of anchoring strength on the ^{2}H-NMR spectrum, we consider the escaped-radial configuration presented in Fig. 1 described by Eqs. (4)–(6). Two orientations of the cylinders in the magnetic field have been considered: the case where the cylinder axis is parallel to the magnetic field ($\theta_B=0°$), and the case where the cylinder axis is perpendicular to the magnetic field ($\theta_B=90°$). Several values of the dimensionless variable σ were used to simulate ^{2}H-NMR spectra for the two orientations of the cylinder in the magnetic field. The results of this simulation are presented in Fig. 3. First consider the spectra where $\theta_B=0°$ and $\sigma=\infty$, which correspond to the strong-anchoring case where the directors are anchored perpendicular to the surface. The singularities in the spectral pattern correspond to the contribution from molecules whose director is oriented at an angle $\theta=90°$, and the orientation with $\theta=0°$ contributes to the intensity at the shoulders. As σ decreases, the directors at the surface begin to tilt away, resulting in the peaks being shifted to smaller angles towards the center of the spectrum. There also is an increased number of molecules parallel to the cylinder axis, increasing the intensity at the shoulders. In the $\theta_B=90°$ case, a decrease in σ results in a decrease of intensity at the shoulders, shifting them into the 90° singularities. In the trivial case $\sigma\leq1$, where the directors align parallel to the cylinder axis, the $\theta_B=0°$ orientation results in two sharp singularities separated by $\delta\nu_B$, and the $\theta_B=90°$ orientation results

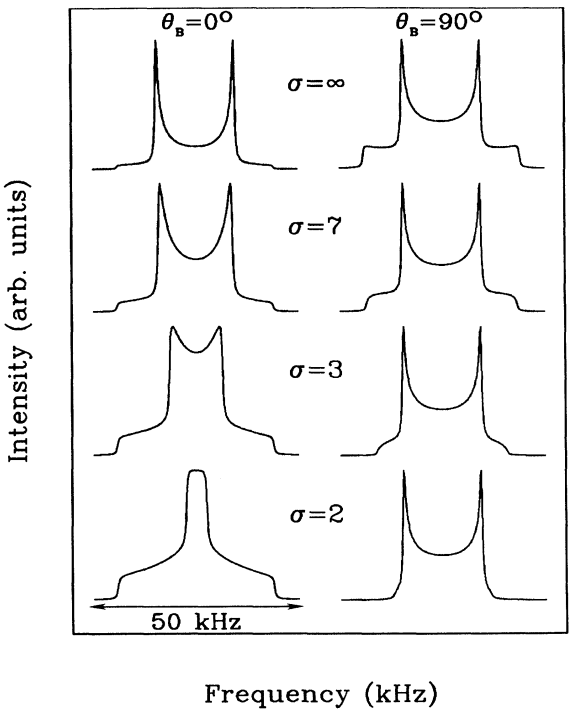

FIG. 3. Simulated ^{2}H-NMR spectral patterns of the escaped-radial configuration without point defects for different values of σ for the cylinder axes parallel, $\theta_B=0°$, and perpendicular, $\theta_B=90°$, to the magnetic field.

in two singularities separated by $\frac{1}{2}\delta\nu_B$ exactly following the angular dependence of Eq. (7). These calculated spectra clearly show the sensitivity of the ^{2}H-NMR technique to the effective molecular-anchoring strength in liquid-crystal dispersed systems with cylindrical symmetry.

There are several ways to vary the parameter σ: the surface can be treated to change the molecular-anchoring strength; a liquid-crystal material can be chosen whose effective elastic constant changes as a function of temperature; a liquid-crystal material can be used with a different K_{24}; or the curvature can be varied by employing various cylinder sizes. In our experiments we have investigated various cylinder sizes leaving K, K_{24}, and W_0 unchanged. Thus the spectral pattern can be simulated for various cavity sizes and W_0 and K_{24} can be determined. In our experimental system, singular point defects exist and must be included in the line-shape calculation.

IV. EXPERIMENTAL METHOD

The confining geometries used in our studies were prepared by filling the cylindrical channels of Nuclepore membranes [24] with the liquid-crystal compound 4′-pentyl-4-cyanobiphenyl deuterated in the β position of the hydrocarbon chain (5CB-βd_2). The purity of the 5CB-βd_2 was measured to be 99.6% using high-pressure liquid chromatography [25]. The Nuclepore membrane is composed of a polycarbonate film with cylindrical pores penetrating through its 10-μm thickness. The pores are well-defined cylinders oriented perpendicular to the surface of the membrane as shown by the scanning-electron-microscope photograph presented in Fig. 4. Four pore sizes were used in our studies, 0.3, 0.2, 0.1, and 0.05 μm in radius. The membranes are principally used in critical filtration processes [26], but have found applications in other disciplines such as low-temperature physics [27]. The characterization and application of these membranes has been discussed in the literature [28,29].

The membranes are initially cut in 4-mm-wide strips and wetted with a small amount of 5CB-βd_2. To ensure complete wetting, the dispersions are taken into the isotropic phase ($\sim$40° C) for 1 h. The strips are then placed between two Whathan filtration papers for several minutes to remove any remaining liquid crystal from the membrane surface. Approximately 200 strips are uniformly stacked and placed in a 5-mm-diam NMR tube which yields a sufficient signal for NMR experiments. The experiments were performed on a home-built coherent-pulse spectrometer specifically designed for phase-transition studies and phase-structure determination of liquid-crystalline materials. A modified quadrupolar echo sequence $(\pi/2)_x$-τ-$(\pi/2)_y$ was used where $\tau = 100$ μs and the length of each of the $\pi/2$ pulses was 5 μs. The shorter values of τ (down to 40 μs) left the spectral line shape unchanged. The free-induction decay was averaged 10 000–30 000 times depending on the cylinder size. The smaller cylinder sizes require additional averaging because less deuterated material is present in the sys-

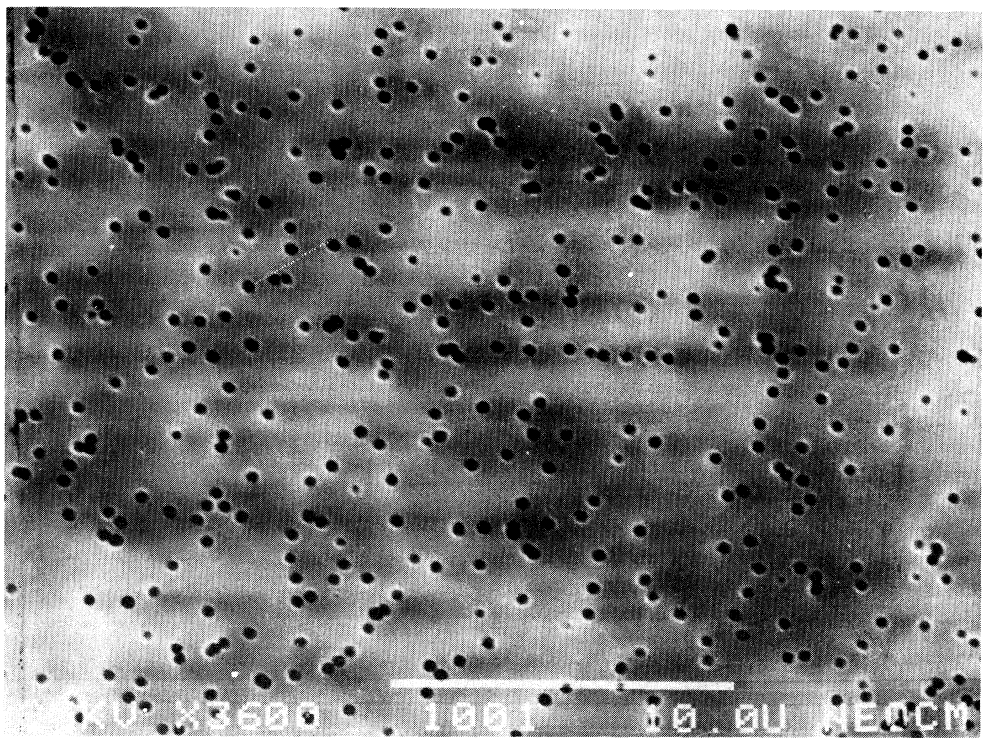

FIG. 4. Scanning electron microscopic photograph of a polycarbonate Nuclepore membrane with cylindrical cavities of radius 0.3 μm. The scale shown in the photograph is 10 μm.

tem. The temperature resolution of the instrument is 0.1 °C and the orientation of the sample can be controlled to within 0.05°. The sample is placed in the magnetic field such that the cylinder axes are parallel to the field and can be rotated to a position where the cylinder axes are perpendicular to the field.

V. EXPERIMENTAL RESULTS AND COMPARISON WITH THEORY

The ^{2}H-NMR spectra were measured at 9 °C below the nematic-isotropic transition temperature for four different cavity sizes at two sample orientations, and are presented in Fig. 5. The quadrupole splittings of the experimental spectra are normalized to the bulk nematic splitting frequency, so the spectral shapes can be compared for all cylinder sizes. This corrects for the effect of diffusion, which slightly shifts the peaks but has no influence on the shape of the spectral pattern for these cavity sizes [9]. The largest cavity size studied, $R=0.3$ μm, has been analyzed in detail in a previous paper [9]. It was shown that the ^{2}H-NMR spectral pattern corresponds to the escaped-radial structure with a linear array of singular point defects. For the parallel cylinder orientation there are two peaks (which are separated by $\frac{1}{2}\delta\nu_B$) that arise from molecules anchored perpendicular to the surface. The spectral shape at $\theta_B=90°$ is similar to the

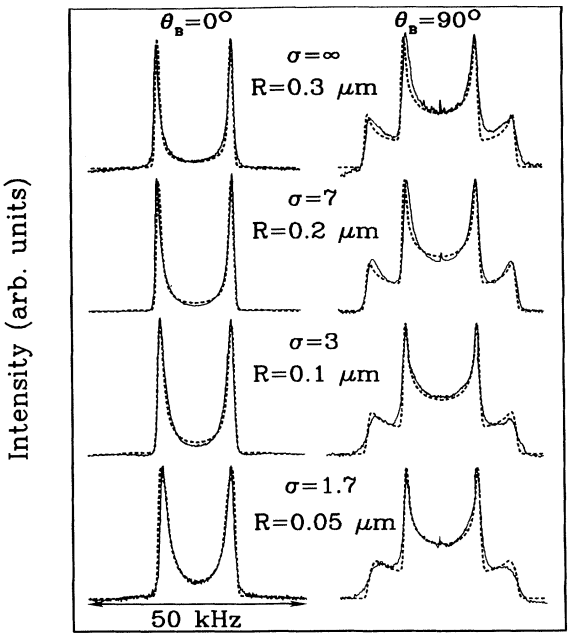

FIG. 5. Experimental ^{2}H-NMR spectra of 5CB-βd$_2$ confined in Nuclepore membranes recorded at 9° below the nematic-isotropic transition temperature for four different cavity sizes at the $\theta_B=0°$ and 90° orientations of the cylinder axes in the magnetic field. The dashed curve represents theoretical fits calculated for each cavity size and the corresponding value of σ which gives the best fit for $L/R=1.5$.

cholesteric pattern [30] with director orientation isotropically distributed in the plane of the magnetic field, but with smaller outer peaks in view of the escape along the cylinder axis. Detailed analysis showed that the defects along the cylinder axis must not be neglected. The average distance between the defects was found to be $L=(2\pm0.5)R$ [9].

As the cavity radius is decreased, the spectra can reflect some changes in the molecular structure and dynamics as will now be discussed. A continuous transition occurs from a strong-anchoring regime with $\sigma\gtrsim10$ to a weak-anchoring regime $\sigma\leq1$ at small radii where the anchoring angle deviates from 90°. Here two defect structures are possible, one with alternating radial and hyperbolic defects as in the strong-anchoring case, and one with only hyperbolic defects [20]. The stability of the defect structure depends on the value of L/R. It has been predicted theoretically that under strong-anchoring conditions a configuration transition from escaped radial to planar radial with an isotropic core along the cylinder axis will occur when R becomes smaller than a critical value $R_c\sim0.1$ μm[1,2]. It will be shown, however, that weak-anchoring energies prevent this transition from occurring in samples studied here. There is no evidence that that NMR is sensitive to the diminished molecular order and biaxiality [31] expected to exist in the vicinity of defects.

The spectral line shape at the $\theta_B=0°$ orientation in Fig. 5 shows little dependence on the radius in larger cavities, but for $R=0.05$ μm shoulders begin to appear and the central portion of the spectrum becomes higher. The relatively low central part is an indication of alternating radial and hyperbolic defects with the average defect density L/R between 1 and 2. The ratio L/R depends on the sample, as the onset of these defects is a result of wall irregularities, and is not intrinsic to the liquid-crystal material [9]. There has been no experimental observation of the structure with only hyperbolic defects, which would be manifested in the appearance of two side peaks at the bulk nematic-liquid-crystal frequency. Otherwise, the $\theta_B=0°$ spectra are not sensitive to the value of σ when the defects are present. On the other hand, the $\theta_B=90°$ orientation is sensitive to the magnitude of σ for all defect densities larger than $L/R\sim1.2$. We have simulated the experimental ^{2}H-NMR spectra in Fig. 5 (dotted curve) using the value of σ as the only fitting parameter at a constant average defect density $L/R\sim1.5$.

The fitted values of the surface parameter σ are presented in Fig. 6 for cavities of radius 0.3, 0.2, 0.1, and 0.05 μm respectively. The $R=0.3$ μm sample is already in the strong-anchoring limit and therefore we can only measure a lower bound for σ. The molecular-anchoring strength W_0 and the surface elastic constant K_{24} are determined from the graph of σ versus radius (see Fig. 6). This results in a linear relationship where W_0/K is the slope and $K_{24}/K-1$ is the ordinate intercept. Our fits yield values of $W_0/K=3.5\times10^7$ m^{-1} and $K_{24}/K\approx1$. The anchoring strength W_0 is found to be $\sim2.5\times10^{-4}$ J/m^2 using the value $K=7\times10^{-12}$ J/m. The surface extrapolation length defined as $d_e=K/W_0$ is calculated to be 28 nm.

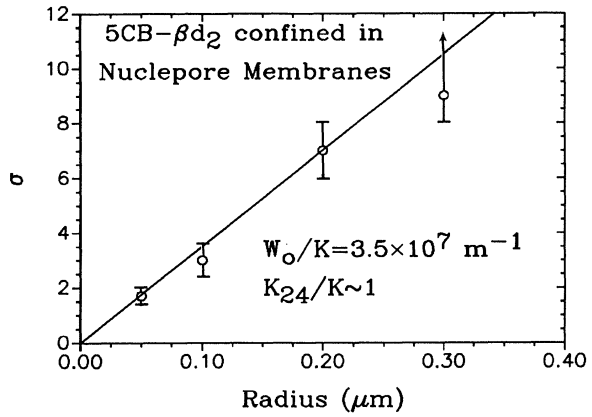

FIG. 6. The effective anchoring strength as a function of radius. W_0/K and $K_{24}/K-1$ are given by the slope and ordinate intercept of the solid line, respectively.

Preliminary calculations [32] show that the effect of the translational diffusion on the $\theta_B=90°$ spectrum is first a decrease in the distance between the singularities, and then an increase in the intensity in the shoulder and the central part of the spectrum. A comparison with experimental data shows that the influence of diffusion is relatively small, shifting the $\theta=90°$ singularities by $\sim 20\%$ for the smallest cavity size studied. This indicates that the actual value of the diffusion constant in smaller cylinders is decreased, probably as a result of increased curvature. It has been shown in chiral systems that twist deformations can lower the diffusion rate [33].

We did not observe any transition between the escaped-radial with singular point defects and the planar-radial configuration in the cavity sizes used in this study. Of course this transition was considered only in the strong-anchoring approximation and must be extended to the finite-anchoring case.

VI. CONCLUSIONS

We have extended the understanding of the escaped-radial configuration to cases where anchoring considerations and surface elastic terms in the elastic free energy become important. The ^{2}H-NMR technique and compact cylindrical geometry of polycarbonate Nuclepore membranes allow the determination of the director configuration and measurement of W_0 and K_{24} in submicrometer cavities not accessible before. We have yet to observe the predicted configuration transitions from the escaped radial to planar radial, which may never be detectable because of finite-anchoring energies. It is a subject of future work to investigate the role of terms in the elastic free energy, such as K_{13}, and others that involve the square of the second derivatives of **n**. These terms may be of significance, but it is not a trivial problem and is beyond the scope of this paper. There are many things yet to be done experimentally such as exploring different preparations of the cavity surface with various polymers and surfactants [34], and exploring the effect of the splay-to-bend ratio on the director configuration [35]. Tangential anchoring conditions are also of interest. In this case the twist constant K_{22} is expected to be of importance and molecular anchoring becomes more complicated.

ACKNOWLEDGMENTS

The authors acknowledge the support of the National Science Foundation (NSF) under Solid-State Chemistry Grant No. DMR88-17647, the NSF Science and Technology Center ALCOM DMR89-20147, the Slovenian Research Foundation, and the NSF Joint Fund Project 795, "Composite Liquid Crystals," INT 87-21016. The deuterated compound was synthesized by Sandra Keast under the support of the National Center for Integrated Photonic Technology (NCIPT) Contract No. MDA972-90-C-0037.

[1] P. E. Cladis and M. Kleman, J. Phys. (Paris) **33**, 591 (1972).
[2] R. B. Meyer, Philos. Mag. **27**, 405 (1973).
[3] C. E. Williams, P. Pieranski, and P. E. Cladis, Phys. Rev. Lett. **29**, 90 (1972).
[4] P. G. de Gennes, *The Physics of Liquid Crystals* (Clarendon, Oxford, 1974).
[5] C. Williams, P. E. Cladis, and M. Kleman, Mol. Cryst. Liq. Cryst. **21**, 355 (1973).
[6] M. Kleman, *Points, Lines, and Walls in Liquid Crystals, Magnetic Systems, and Ordered Media* (Wiley, New York, 1988).
[7] A. Saupe, Mol. Cryst. Liq. Cryst. **21**, 211 (1973).
[8] H. Lin, P. Palffy-Muhoray, and M. A. Lee, Mol. Cryst. Liq. Cryst. **198**, 55 (1991).
[9] G. P. Crawford, M. Vilfan, I. Vilfan, and J. W. Doane, Phys. Rev. A **43**, 835 (1991).
[10] D. Riviere, Y. Levy, and E. Guyon, J. Phys. (Paris) Lett. **40**, L-215 (1979).
[11] H. Yokoyama and H. A. van Sprang, J. Appl. Phys. **57**, 4520 (1985).
[12] H. Yokoyama, S. Kobayenkov, and H. Kamei, J. Appl. Phys. **61**, 4501 (1987).
[13] L. M. Blinoff, A. Yu. Kabayenkov, A. A. Sonin, Liq. Cryst. **5**, 645 (1989).
[14] J. H. Erdmann, S. Zumer, and J. W. Doane, Phys. Rev. Lett. **64**, 1907 (1990).
[15] J. W. Doane, A. Golemme, J. L. West, J. B. Whitehead, Jr., and B. G. Wu, Mol. Cryst. Liq. Cryst. **165**, 511 (1988).
[16] J. W. Doane, N. A. Vaz, B. G. Wu, and S. Zumer, Appl. Phys. Lett. **48**, 269 (1986).
[17] M. Kuzma and M. M. Labes, Mol. Cryst. Liq. Cryst. **100**, 103 (1983).
[18] G. P. Crawford, D. K. Yang, D. Finotello, S. Zumer, and J. W. Doane, Phys. Rev. Lett. **66**, 723 (1991).
[19] M. Vilfan, V. Rutar, S. Zumer, G. Lahajnar, R. Blinc, J. W. Doane, and A. Golemme, J. Chem. Phys. **89**, 579 (1988).
[20] I. Vilfan, M. Vilfan, and S. Zumer, Phys. Rev. A **43**, 6875 (1991).

[21] A. Golemme, S. Zumer, and J. W. Doane, Phys. Rev. A **37**, 559 (1988).
[22] J. W. Doane, in *Magnetic Resonance of Phase Transitions,* edited by F. J. Owens, C. P. Poole, Jr., and H. A. Farach (Academic, New York, 1979), Chap. 4.
[23] A. Abragam, *The Principles of Nuclear Magnetism* (Oxford University Press, London, 1961).
[24] Nuclepore Corporation, 7035 Commerce Circle, Pleasanton, CA 94566.
[25] S. Keast and M. Neubert (private communication).
[26] J. C. Moore (unpublished).
[27] F. M. Gasparini, G. Agnolet, and J. D. Reppy, Phys. Rev. B **29**, 138 (1984).
[28] T. Chen, M. J. Dipirro, B. Bhattacharyya, and F. M. Gasparini, Rev. Sci. Instrum. **51**, 846 (1980).
[29] M. C. Porter (unpublished).
[30] G. Chidichimo, Z. Yaniv, N. P. Vaz, and J. W. Doane, Phys. Rev. A **25**, 25 (1982).
[31] N. Schopohl and T. J. Sluckin, Phys. Rev. Lett. **59**, 2582 (1987).
[32] S. Kralj, M. Vilfan, and S. Zumer (unpublished).
[33] R. Stannarius, Liq. Cryst. **8**, 389 (1990).
[34] G. P. Crawford, D. W. Allender, and J. W. Doane (unpublished).
[35] R. Ondris-Crawford and J. W. Doane (unpublished).

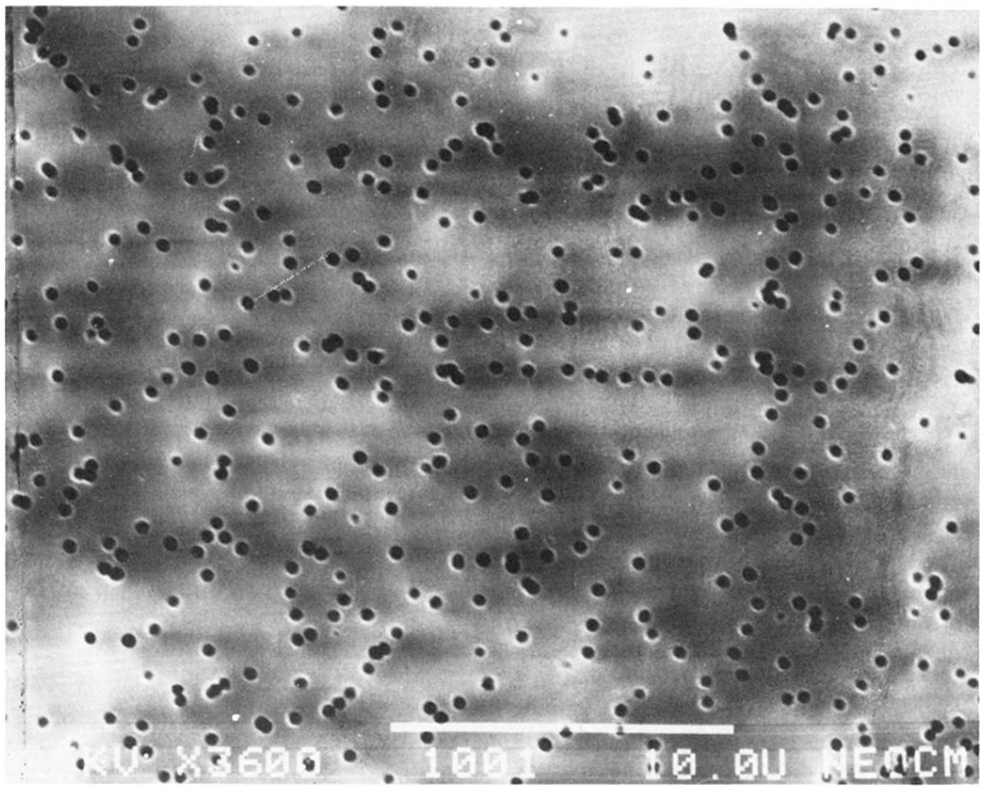

FIG. 4. Scanning electron microscopic photograph of a polycarbonate Nuclepore membrane with cylindrical cavities of radius 0.3 μm. The scale shown in the photograph is 10 μm.